J. Earth Syst. Sci. (2022)131 207
https://doi.org/10.1007/s12040-022-01960-8

Strength enhanced by pseudotachylite melt in fault zone rocks during post-seismic melting: A case study from the Gangavalli fault zone, southern India

Bhuban Mohan Behera[1,*], Ashutosh Tripathy[2] and Tapas Kumar Biswal[1]

[1]*Department of Earth Sciences, Indian Institute of Technology Bombay, Powai, Mumbai 400 076, India.*
[2]*Department of Applied Geology, Indian Institute of Technology (Indian School of Mines), Dhanbad, Dhanbad, Jharkhand 826 004, India.*
**Corresponding author. e-mail: beherabhubanmohan@gmail.com*

MS received 27 November 2021; revised 30 April 2022; accepted 5 May 2022

Evidence of frictional melting in the form of pseudotachylite is innumerably found along the Gangavalli fault zone (GFZ), southern India. Such catastrophic deformation influences the strength of rock masses across the fault zone. In this paper, we have investigated the strength variation in fault zone rocks during post-seismic deformation. The experimental study suggests that the average uniaxial compressive strength (UCS) for pseudotachylite hosting charnockite (i.e., Pt-charnockite) is almost double (45.58 MPa) as compared to the pseudotachylite devoid charnockite (i.e., D-charnockite) of 24 MPa. The melt associate seismic deformation shows high stress drop due to melt lubrication at the fault interface and simultaneously produced numerous fractures in the rock. We have determined the stability and denseness of both rock types using acoustic emission (AE) technique that remarks a distinct difference in AE signatures. The analysis indicates a more stable and dense Mogi type-III signature for post-seismic deformed rocks that are assisted by pseudotachylite melt. However, negligible AE energy is observed in the D-charnockite. We proposed that the melt-assisted seismic deformations are more inhibitable to reactivate the slip surfaces than the conventional earthquake-deformed rock having no melting phenomenon and therefore, pseudotachylites enhance the strength of fault zone rocks during post-seismic deformation.

Keywords. Fault zone rock; pseudotachylites; seismic faulting; acoustic emission; uniaxial compressive test; Gangavalli fault zone.

1. Introduction

Fault-generated pseudotachylites are produced by high-speed friction along the fault interface. This rapid brittle deformation associated with pseudotachylite veins builds many flaws in the surrounding country rock in the form of fractures, breccia, ultra/cataclasites, gouges, offset markers and slip surface. These features are undoubtedly recognised as deformation markers that reduce the strength of upper crustal rocks, whereas pseudotachylite melt, a seismogenic marker contradicts the former opinion of rheological distribution across the fault zone rocks. Previous workers have focused on strength analysis of samples that are devoid of naturally occurring pseudotachylite using laboratory set-up to produce frictional melt (Proctor and Lockner 2016). In this study, we have attempted strength

Published online: 24 September 2022

analysis on natural pseudotachylite samples and compared them with pseudotachylite-free samples during post-seismic deformation. The Gangavalli fault zone (GFZ) in the Southern Granulite Terrane (SGT) in India (figure 1) hosts many pseudotachylite veins emplaced into fracture openings (Behera *et al.* 2017) and hence, this area is best suited for the analysis.

Observation of strength due to presence of pseudotachylite in the fault zone rocks has evolved almost a decade ago (Proctor and Lockner 2016). Few researchers have reported an increase in post-seismic strength of pseudotachylite-bearing fault rock (Proctor and Lockner 2016) through experimental analysis by producing frictional melt and considering them as pseudotachylite. Mitchell *et al.* (2016) have pointed out that the lubrication effect of frictional melt at the onset of deformation makes rapid slip along fault interface. While after solidification, the hot frictional melt increases the strength of weak zones. Beeler *et al.* (2016) have documented pseudotachylite as a paleoearthquake source rock properties describing co-seismic fault strength and stress drop at static conditions. The stress drops for minor earthquake faulting (which is not capable of producing melt) are less compared to the large earthquake. Therefore, it can be stated that the stress drop is more for a pseudotachylite-linked earthquake faulting than non-pseudotachylite earthquake faulting (McKenzie and Brune 1972). Many authors have determined the shear stress resistance of pseudotachylite-linked fault rocks using field data of fault vein thickness (i.e., thickness of pseudotachylite veins along the fault plane) and displacement of offset markers (Sibson 1975; Barker 2005; Di Toro *et al.* 2005; Beeler *et al.* 2016; Behera *et al.* 2020). Contrarily, the basalt hosting pseudotachylite at shallow subduction complex decreases the post-seismic strength of fault rock where an alteration to phyllosilicate is caused by dehydration (Phillips *et al.* 2019). However, the measurement of post-seismic strength of natural pseudotachylite samples is challenging, particularly during the sample preparation, because pseudotachylites are glassy/fragile and easily break into pieces. A comparative study of fault damage rocks with and without pseudotachylite melt still carries a lot of scope for more study. In this paper, we have demonstrated fracturing in fault zone rocks with and without pseudotachylite veins during post-seismic melting. This will help to understand the mechanical behaviour of rock during post-seismic deformation and the role of pseudotachylite melt in strengthening the weak fault zone rocks.

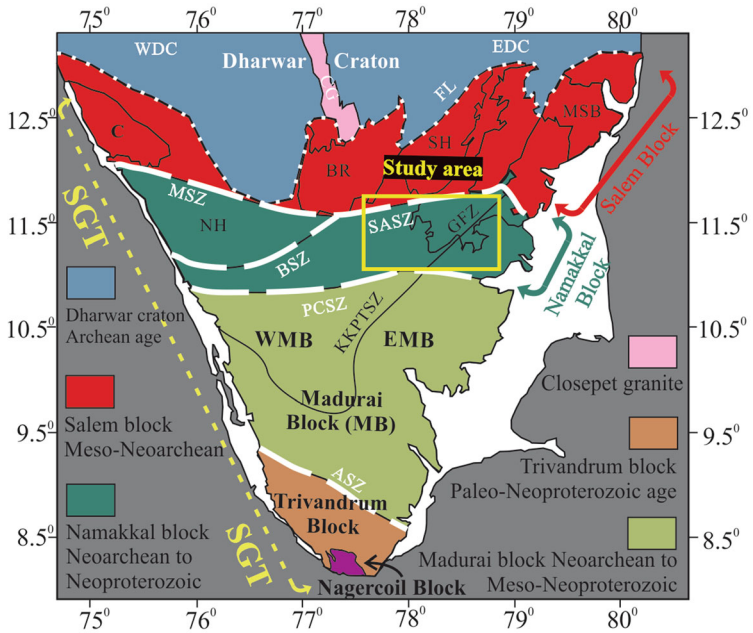

Figure 1. Geological map of Southern Granulite Terrane (SGT) (Ramakrishnan and Vaidyanadhan 2008) with major blocks and shear zones. ASZ: Achankovil Shear Zone, BR: Biligirirangan, BSZ: Bhabani Shear Zone, C: Coorg, CG: Closepet Granite, EDC: Eastern Dharwar Craton, FL: Fermor's Line, KKPTSZ: Karur–Kambam–Painavu–Trichur Shear Zone, MSB: Madras Block, MSZ: Moyar Shear Zone, PCSZ: Palghat–Cauvery Shear Zone, SASZ: Salem–Attur Shear Zone, SH: Shevroy Hill, WDC: Western Dharwar Craton, and GFZ: Gangavalli Fault Zone.

2. Geological background

The southern part of the Indian peninsula is occupied with high-grade granulite rocks and recognised as Southern Granulite Terrane (SGT) with some felsic to mafic/ultramafic intrusive bodies (figure 1). The area is covered with high hills of charnockite plutons and these charnockites are characterised by coarse-grained assemblage of quartz, feldspar, hypersthene, garnet porphyroblasts and carbonate minerals. The mildly developed gneissic impressions are observed as the alternative layers of mafic and felsic minerals. The host charnockite rocks are acidic with high silica content varies from 61.77 to 71.17%, and formed in a dry environment (Behera *et al.* 2020). Structurally, the E–W running km long shear zones across the SGT have divided the terrane into blocks of contrasting structural features, lithology and geochronology (figure 1). The study area, the Gangavalli fault zone (GFZ), is located south of the Salem–Attur shear zone (SASZ) (made of multiple E–W running mylonite zones) (figure 2). This area has been interpreted as part of a positive flower structure resulting from the collision between the Dharwar Craton and the Madurai Block (Chetty *et al.* 2016). The evidence of ductile deformation in the SGT is well presented by the network of deep crustal shear zones. However, some brittle deformations (i.e., in the form of normal faulting at 0.8–0.5 Ga; Behera *et al.* 2019) are also documented as younger events or late phase of deformation in the terrane. Older ages of brittle deformations are seldom reported in the geological records of the SGT. Evidence of brittle deformation in mesoscale is found as quartz veins, extensional fractures, pegmatite veins, offset markers, cataclasites, pulverised rock/fault gouges and pseudotachylite veins. The pseudotachylite bearing faults (i.e., the GFZ) represent intense brittle deformation because they are associated with frictional melting along the fault plane (Sibson *et al.* 2006; Kirkpatrick *et al.* 2009; Kirkpatrick and Rowe 2013). The GFZ is an example of such prominent brittle fault in the SGT. The GFZ belongs to the Namakkal Block and truncates against the SASZ (figure 2), which runs about 50 km along NNE–SSW (figure 3). The GFZ dominantly shows a sinistral sense of faulting on a regional scale (Behera *et al.* 2019). However, conjugate fractures

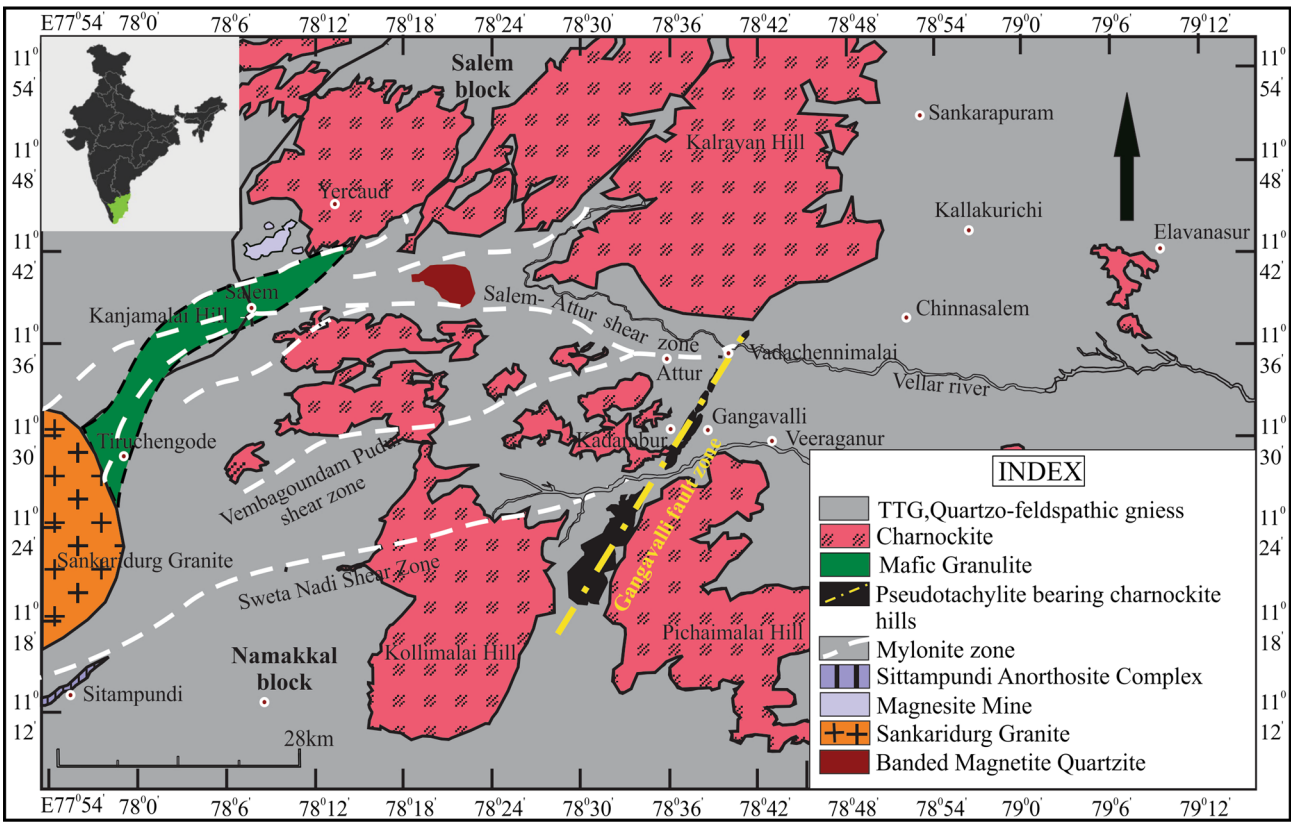

Figure 2. Geological map showing location of the Gangavalli fault zone (yellow dashed line) and major rock types in the Salem–Namakkal block in the Southern Granulite Terrane (SGT) (modified after Sundaralingam *et al.* 2013).

(e.g., oriented along NNE and NW; Behera *et al.* 2017) are present, which locally show both dextral and sinistral sense of shear. The N–S compression has resulted in the sinistral strike–slip faulting known as the Gangavalli strike–slip fault with numerous pseudotachylite veins (figure 3; Behera *et al.* 2017). Pseudotachylites are extensively developed along NNE–SSW strike with subvertical to vertical dip and follow one of the dominant fracture orientations in the GFZ. Although, majority of veins trend NE–SW, they also show wide variation of emplacement into fractures from NE–SW to E–W to NW–SE.

3. Pseudotachylite field observation

Pseudotachylite occurs as dark veins with a sharp cutting edge within the white to pink coloured charnockitic massif (figure 4). These veins are distinct from other mafic veins due to the incorporation of country rock fragments or monomineralic clasts within the matrix. The field study shows that most of the clasts are round to subround, suggesting decrepitation at a high temperature near grain boundary producing a 'quasi conglomerate' or 'false conglomerate' (figure 4a). These veins vary in thickness from few millimetres to tens of centimetres. The melt under high pressure moves towards the opening of low-pressure fractures. At some instants, the melt pressure is so high that it is capable of opening the tightly packed gneissic planes in plausible orientations (figure 4b). The dilation of fractures is also noticed from the 'pinch and swell' feature of the fault veins (figure 4c). This structure could be resulted either due to the viscosity variation of melt within the vein itself or the unevenness of the fault surface (Sibson 1975). The thick, straight and elongated veins produce a tapering end (figure 4d). The driving force at the tip of the vein reduces to zero and arrests the melt movement further. The bifurcation and lensoidal structures of vein are also found in some outcrops (figure 4e, f). Some cross-cutting relations of fracture across pseudotachylite veins are observed in the outcrop (figure 4b, d–f).

Pseudotachylite matrices are ultrafine, grey-brown to dark brown in plane polarised light and isotropic in crossed positions. The size reduction of minerals occurs along pseudotachylite vein margin (figure 5a). The devitrification has been mildly developed at some places in the matrix (figure 5b), and gradation of microlite size distribution is noticed from margin to centre of the vein (figure 5c). Majority of clasts are monomineralic quartz grains and very few plagioclases with lithic fragment of the charnockites. Most of the clasts are sub-round to round caused by decrepitation along the clast's corner. Some of the monomineralic clasts and lithic fragments get fractured during seismic deformation and incorporated within the pseudotachylite vein. The clasts have a wide range of size distribution from ultrafine (in micron size) to very coarse grain (in cm scale) and its distribution follow the 'power law' mechanism (Behera *et al.* 2017).

Melt origin pseudotachylites are associated with many micro crystals known as microlites. Microlites are often noticed in the pseudotachylite vein, which are formed by rapid cooling or quenching (less than a few seconds) of glass. They are indicative of the devitrification process from the glassy groundmass (Sarkar and Chattopadhyay 2020). The dark brown matrices are very prone to produce microlites than the grey-brown. Gradual increases in size (i.e., 30–50 μm) of the microlites are noticed from margin to centre of the vein (figure 5c). Three major types of microlites have been identified from the pseudotachylite vein such as: (i) acicular (figure 5d), (ii) sheaf (figure 5e) and (iii) spherulites or overgrowth microlites (figure 5f). Acicular microlites are needle-shaped and simple group of microlites (figure 5d). Their average size is measured as 25 μm. They show a preferred orientation and wrap around the clasts, thereby indicating their formation during the flow of pseudotachylite melt. Sheaf microlite belongs to the complex spherulite group of microlites. It consists of a central bar (average width 9–10 μm) and plumose fibrous (average length is >50 μm) at both ends (figure 5e). These sheaf microlites are found at the centre of the vein, where complexity in the structure of microlite is more. Overgrowth microlites are also a complex group of microlites. They have two parts: (i) central clast fragment of quartz or feldspar and (ii) radiating crystal fibres from clast (figure 5f). The clasts in the melt act as a nucleation surface for microlites to grow over it.

4. Methodology

The major challenge to measure the strength of natural pseudotachylite-bearing rock is its sample preparation. The vulnerability of breaking into pieces makes it difficult to prepare a standard size and shape for the experiment. The conventional

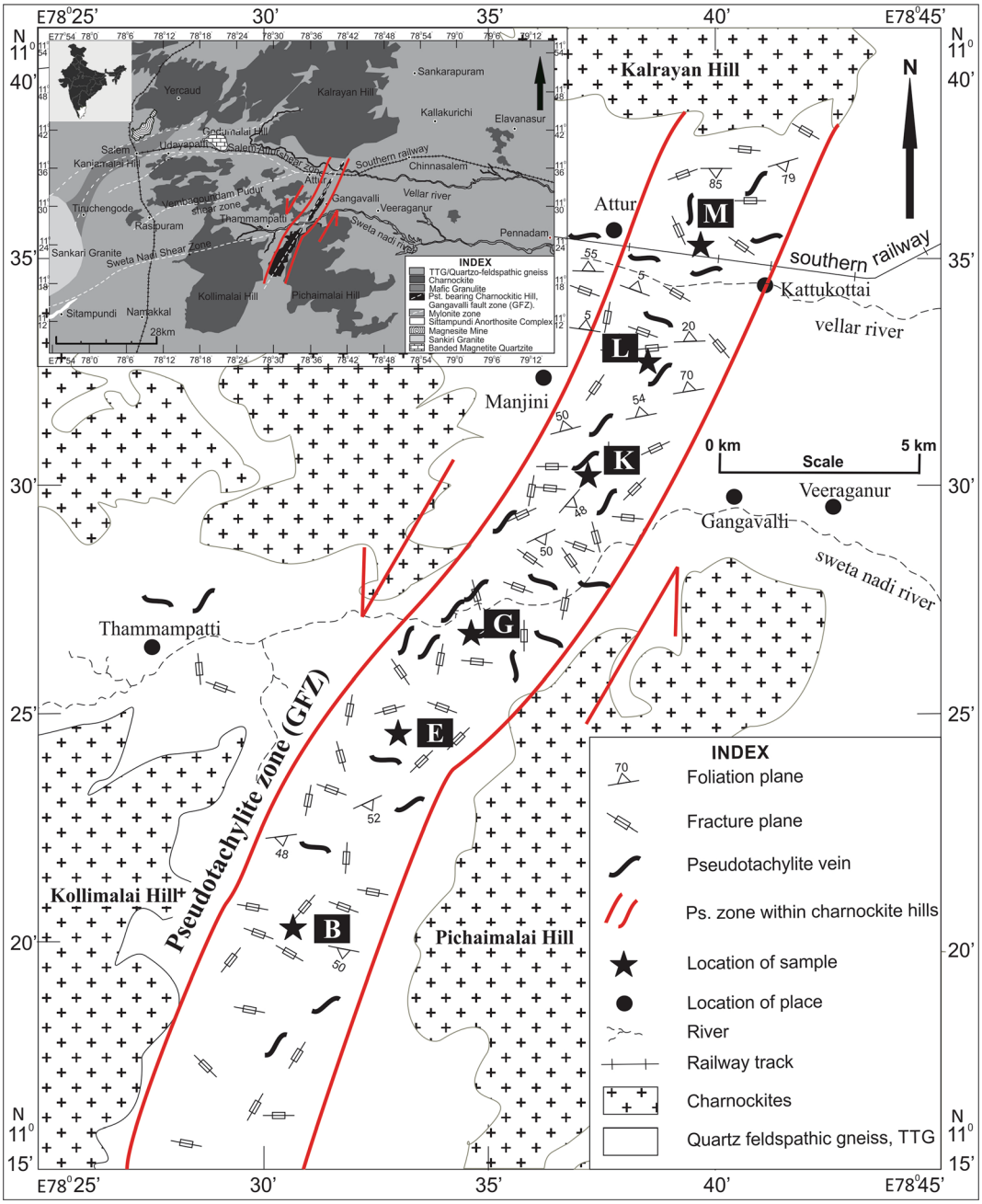

Figure 3. The structural map of Gangavalli fault zone (GFZ). Inset: Regional geological map of Salem–Namakkal block, SGT. Gangavalli fault zone is marked by NE–SW trending pseudotachylite bearing charnockite hills.

way of sample preparation to measure the strength of hard rock requires an NX size core sample of 54.7 mm diameter and diameter to length ratio of 1:2 (ASTM 2001). These difficulties are repeatedly faced during the coring of an NX size sample containing pseudotachylite veins. Therefore, an alternative method of making cubical block samples was adopted for this experiment. Cubes were prepared with face length varying from 38.63 to 48.3 mm for all samples with or without pseudotachylite (figure 6). Similar blocks were also documented by some researchers for petrophysical studies. Sample dimension of 0.8–1.2 cm thick and 5×5 cm^2 area is used by Collettini *et al.* (2009) for analysis. Similarly, Smith *et al.* (2017) have used sample dimension of 1–1.4 cm thickness and 4×4 cm^2 area for direct shear.

Through this experiment, we have tried to acquire the knowledge of fracturing of seismically deformed melt assisted fault rocks and its

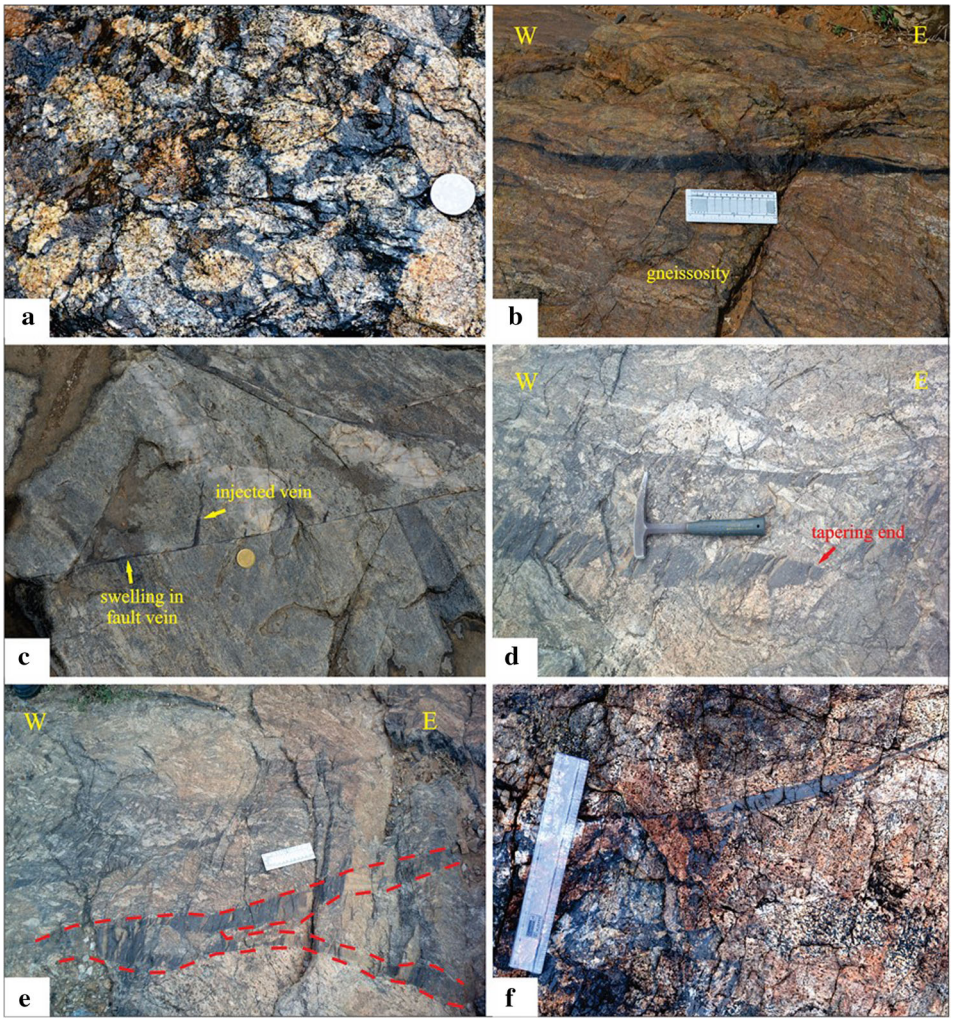

Figure 4. Field photograph of pseudotachylite from the Gangavalli fault zone (GFZ). **(a)** Sub-round to round clasts known as 'quasi conglomerate', **(b)** vein parallel with gneissic plane and the central swelling of the vein with tapering at both ends indicates the dilation, **(c)** fault vein with 'pinch and swell' structures, **(d)** thick injected vein with tapering end, **(e)** bifurcation of vein, and **(f)** lensoidal vein.

strength, stability, and denseness by using acoustic emission (AE) technique and uniaxial compressional strength (UCS) test. These samples have been collected from the Gangavalli fault zone and categorised as pseudotachylite hosting charnockite gneiss (Pt-charnockite gneiss), where these are considered for post-seismic experimental study. Some samples have been collected selectively from the pseudotachylite zone to avoid any inclusion of melt emplacement and categorised as deformed charnockite gneiss (D-charnockite gneiss; sample B and E) (figure 6). All six representative samples (two samples of D-charnockite gneiss, e.g., sample B and E, and four samples of Pt-charnockite gneiss, e.g., sample-G-K-L-M) were tested under room temperature and pressure condition with a constant rate of loading (0.5–1.0 MPa/s). For a comprehensive study, we have tried to keep less variance parameters for the experimental analysis. Therefore, we have only selected those samples which are devoid of fractures (at least invisible to the naked eye). Similarly, gneissic planes are not well developed in these samples so that they could be easily spotted and measured its orientation with the applied loading direction. Samples were mounted with strain gauges to measure the axial strain and two oppositely faced highly sensitive transducers (R6D type) to detect the acoustic signal in the device named AESMART 2000 (figure 7). Pre-amplifier of 40 dB and a front amplifier of 60 dB were attached to the transducer. The accepted range of 20 kHz to 3 MHz was set to filter out the signal. A threshold of 45 dB was taken for consideration

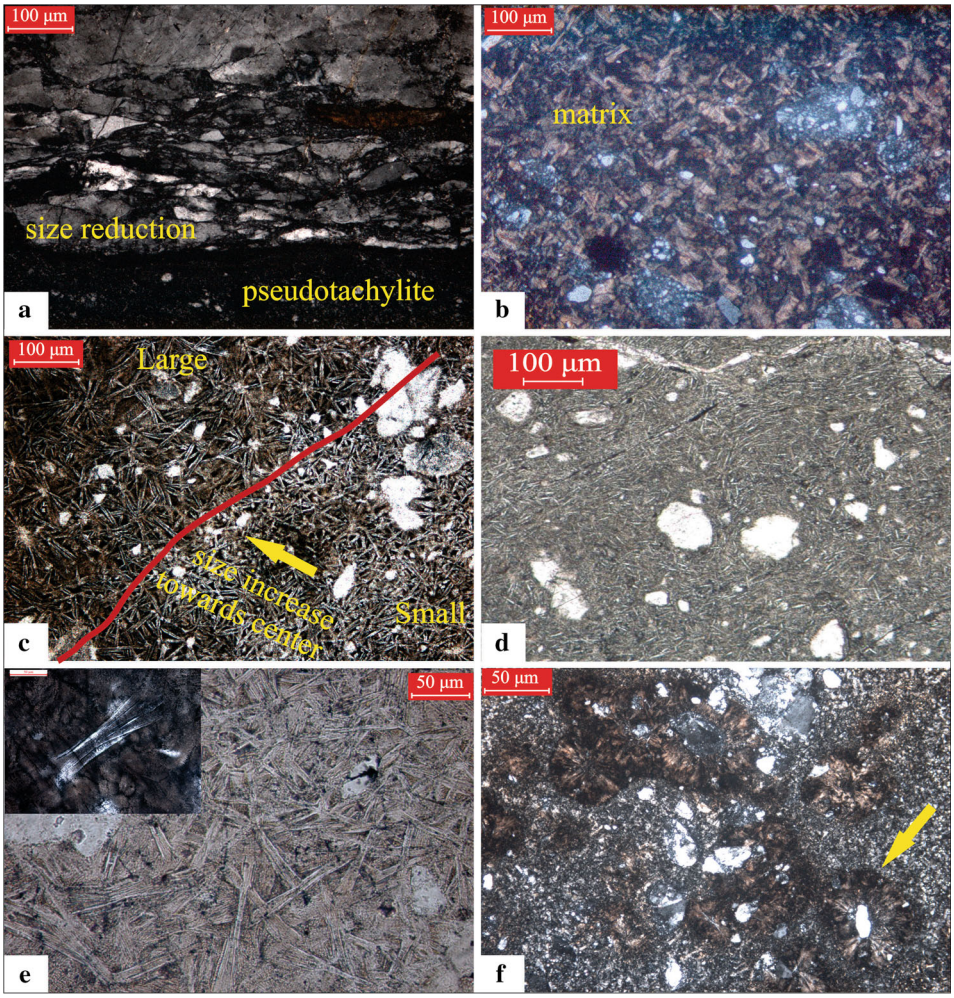

Figure 5. Photomicrographs of pseudotachylite and surrounding country rock. **(a)** Size reduction at the margin of the pseudotachylite vein, **(b)** development of crystallinity in the matrix, **(c)** microlites size increases from margin to center shown by arrow mark, **(d)** needle shaped acicular microlites, **(e)** sheaf microlites (Inset: plumose fibrous structure), and **(f)** overgrowth microlites.

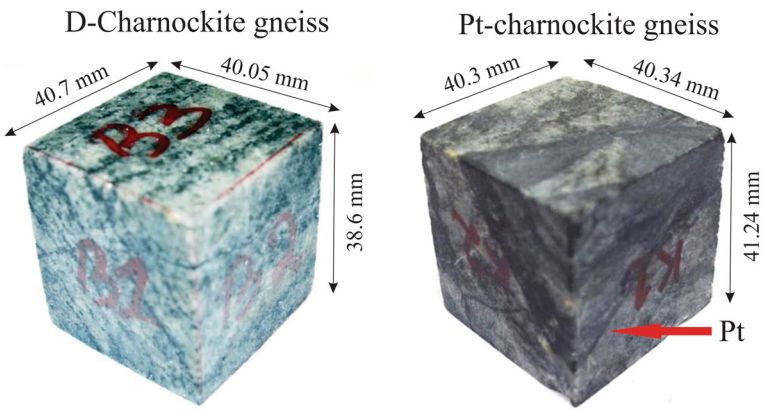

Figure 6. Cubic samples are used for strength analysis for two different rock types, such as deformed charnockite gneiss (D-charnockite gneiss) and pseudotachylite bearing charnockite gneiss (Pt-charnockite gneiss).

of AE analysis with sample frequency of one million samples per second (MSPS). The instrument set-up was the same as Tripathy *et al.* (2018), and the standard method of ISRM (Ishida *et al.* 2017) was followed for the analysis. The results of these two kinds of samples were

compared with those of the fresh charnockite gneiss obtained from the literature study.

5. Results

In this experiment, a remarkable difference in acoustic emission (AE) energy has been noticed between these two rock types. The D-charnockite gneiss shows an early deformation at initial application of stress from 8 to 10 MPa, whereas the Pt-charnockite gneiss starts deforming after 15–20 MPa (figure 8). The maximum peak of AE released during experimental loading on D-charnockite samples is very less as compared to Pt-charnockite gneiss (Y-axis in figure 8). Each zone of AE signal corresponds to a discrete event of deformation in the rock. Samples B and E may not match each other, but they both have low AE peaks as compared to the Pt-charnockite sample. The loading on both samples B and E does not withstand more than 30 MPa of stress unlike Pt-charnockite sample. However, this observation can be grouped under D-charnockite to distinguish both rock types (figure 8). They show a single plane and rapid failure event. In the case of Pt-charnockite gneiss, we observed a wide range of AE energy pulses for these samples caused by progressive propagation of fractures and this broad zone of stress indicates a steady state of deformation.

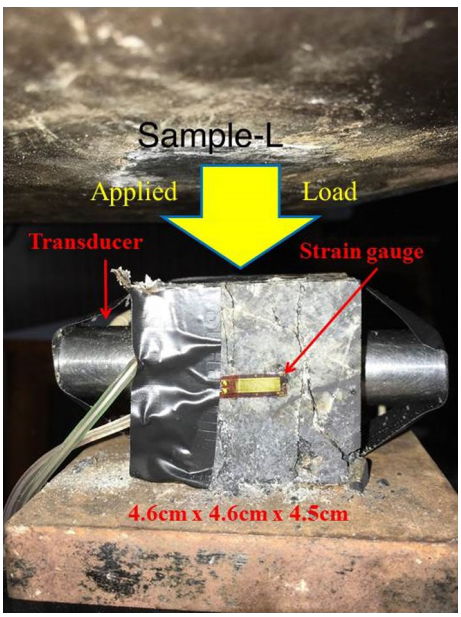

Figure 7. Sample set-up for acoustic emission (AE) as well as uniaxial compressive strength (UCS) test. A constant rate of loading was applied vertically. Two transducers were fitted at oppositely facing sides of the cube and two strain gauges are used at other oppositely faced sides for axial strain measurement.

The nature and stability of rocks across the fault zone can be obtained from Mogi type curve (figure 9; Mogi 1962). The elastic deformation curve (b–c line; figure 9) is nearly horizontal to the abscissa for all samples. During elastic deformation, the material returns to its original state in contrast to plasticity, where the object undergoes permanent change, so it releases negligible amount of acoustic energy (figure 9; horizontal lines suggest elastic deformation). All D-charnockite samples show the presence of crack closure line of Mogi type graph (i.e., a–b line; figure 9). This is due to the fact that the D-charnockite samples possess some pre-existing microcracks or Griffith cracks which are always present in all natural samples and randomly oriented before loading. The open spaces within these microcracks have been closed during the initial application of load on the sample and release comparatively less amounts of AE signals. In samples B and E, the a–b line shows the onset of loading where some of AE counts are released due to closing of microcracks before attending the elastic stage (i.e., line b–c, where AE is rarely released since no permanent deformation occur). But here in sample B, the b–b dash line shows release of notable amount of AE counts before attending elastic stage could be resulted due to presence of a large opening space/weak surface (b–b line in figure 9). However, a field of stable crack propagation (i.e., c–d line; figure 9) is completely missing in these samples. Therefore, D-charnockite samples are considered as not dense and unstable, corresponding to a Mogi type-II (refer to Boyce *et al.* 1981). The Pt-charnockite samples show identical results (figure 9) that indicate the presence of the c–d line of stable crack propagation with maximum energy released. This corresponds to Mogi type-III, which shows dense and stable type samples (figure 9).

The uniaxial compressive strength (UCS) test for these block samples was done simultaneously with the AE testing (figure 7). Considering $\sigma_2 = \sigma_3 = 0$ for the uniaxial test, the obtained failure load is considered as the maximum strength (σ_1) of the rock. Using maximum load (σ_1) and the breaking angle with loading direction (θ), we have calculated shear (τ), normal (σ_n) and cohesion (C) strength, where the angle of internal friction $\phi = 30°$ is taken for most hard rock. The equations used for calculation in the 'MohrPlotter' software are given below.

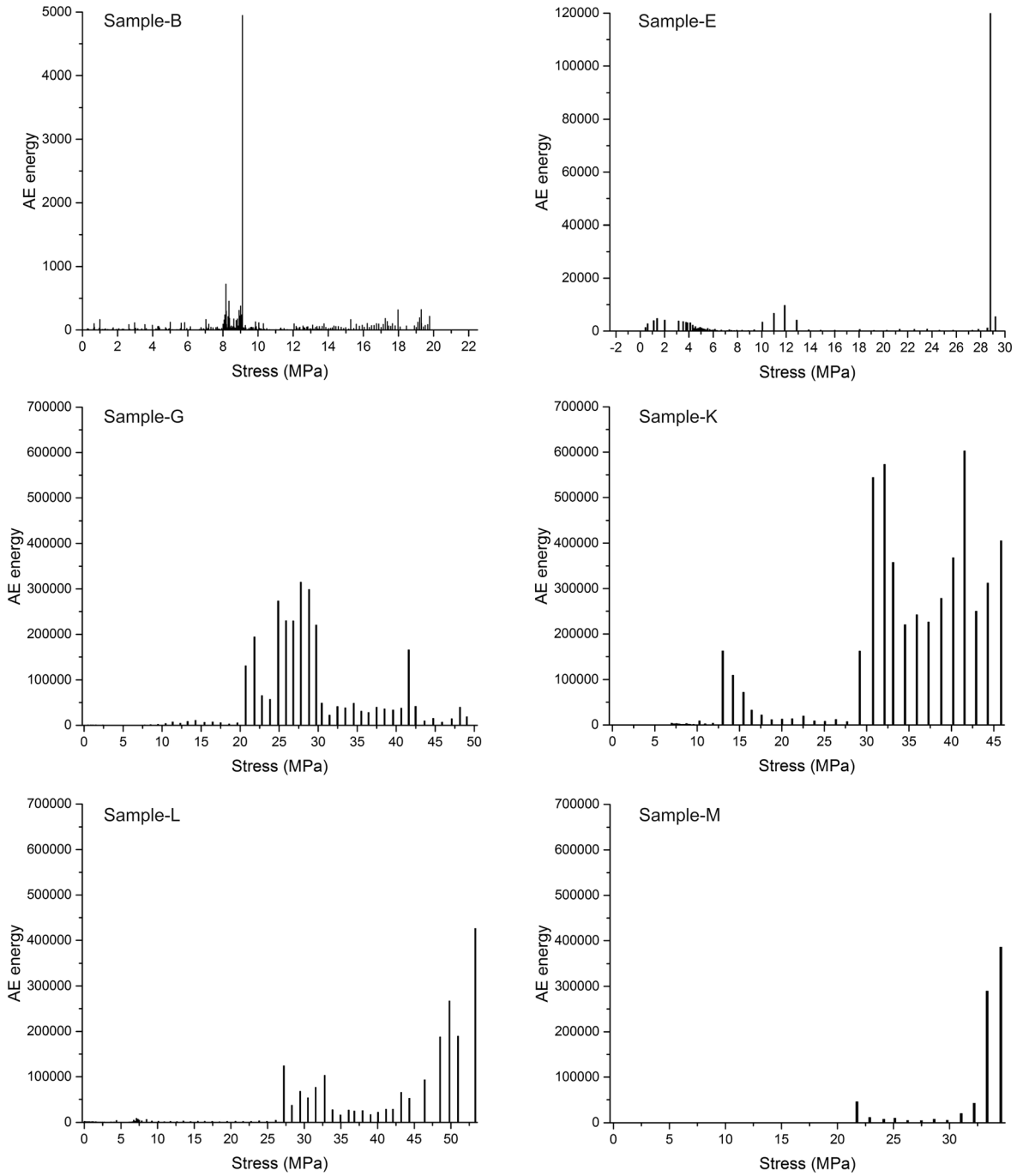

Figure 8. Diagram showing the plot between applied stress *vs.* AE energy for both D-charnockite (Sample-B and E) and Pt-charnockite samples (Sample-G, K, L and M).

$$\tau = \frac{\sigma_1}{2} \times \sin 2\theta, \tag{1}$$

$$\sigma_n = \frac{\sigma_1}{2} - \frac{\sigma_1}{2} \cos 2\theta, \tag{2}$$

$$\tau = \sigma_n \times \tan \phi + C \quad (\phi = 30^\circ \text{ for hard rock}). \tag{3}$$

The UCS results show a major difference in the failure strength (σ_1) for both rock types. All D-charnockite gneisses exhibit less compressive strength (e.g., UCS 19–29 MPa, table 1) as compared to Pt-charnockite gneiss (e.g., UCS 34.61–53.3 MPa, table 1; figure 10). The minimum and maximum values for D-charnockite gneiss are 19 and 29 MPa, respectively (table 1) with an average of 24 MPa. All samples produce clearly visible straight fracture plane/s (i.e., Mode-I) at low angle to the direction of loading (figure 10). All D-charnockite

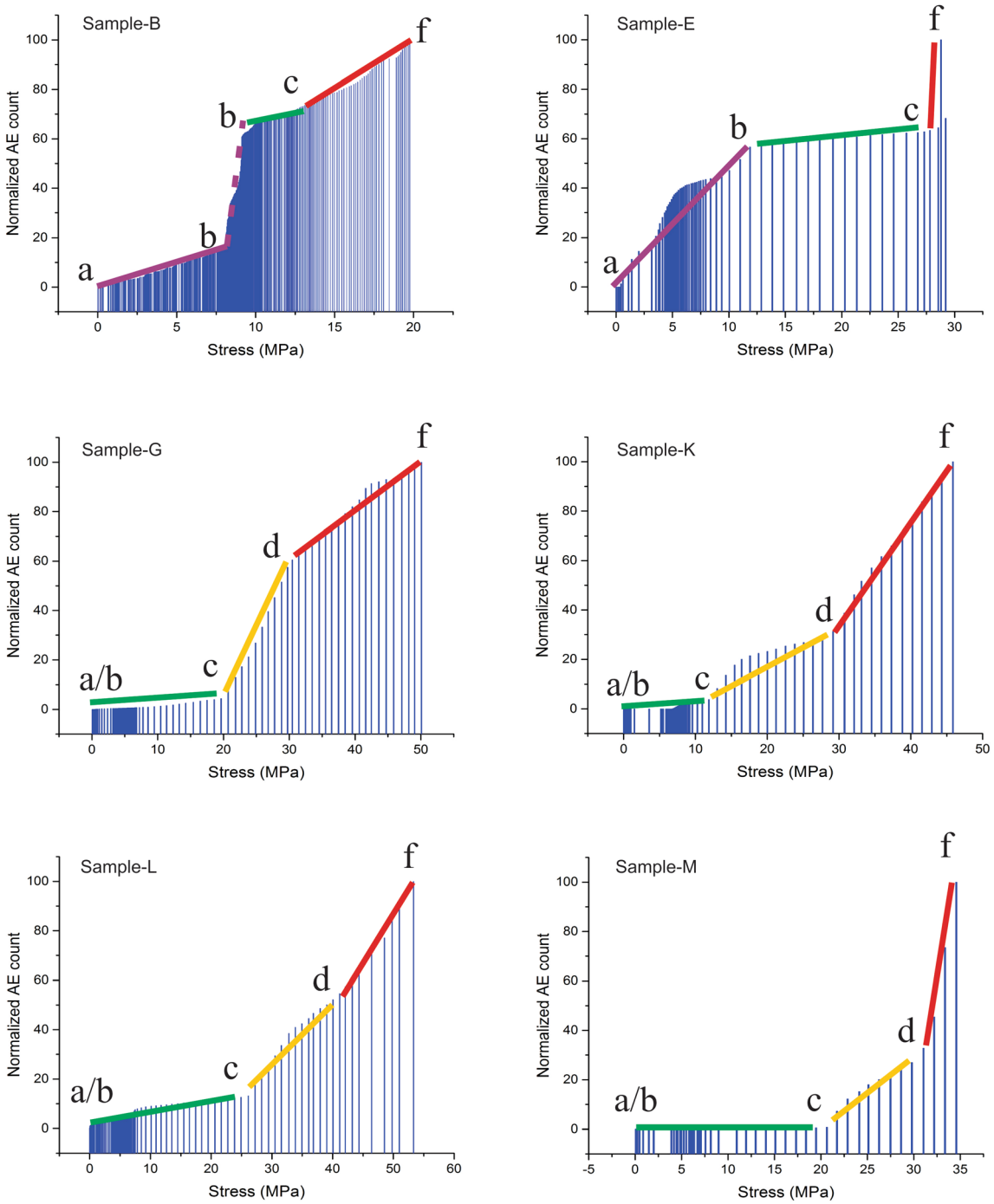

Figure 9. Diagram show the Mogi-type plots between stress *vs.* normalised AE counts. Note: a–b = crack closure, b–c = elastic deformation, c–d = stable crack propagation, d–f = unstable crack propagation, and f = final failure.

samples were broken nearly parallel to the axis of loading with an average angle of $\theta = 10°$ (figure 10). Using the angle of internal friction $\phi = 30°$ for hard rock, we have determined shear strength, normal strength and cohesion of D-charnockite and Pt-charnockite samples (see table 1). The average σ_1 and cohesion for Pt-charnockite are 45.58 and 8.15 MPa, respectively. These values are larger than those of D-charnockite gneiss.

6. Discussion

The samples were subjected to a constant rate of loading (0.5–1.0 MPa/s) to determine UCS value as well as AE counts and energy in tandem. The analysis shows different acoustic responses and fracturing mechanisms for the two rock types, i.e., D-charnockite gneiss (samples B and E) and Pt-charnockite gneiss (samples G, K, L and M). The

maximum number of AE bursts suggests greater degree of heterogeneity (i.e., internal lattice defects, microcracks, degree of impurities, etc.) present in the sample. There are multiple rises of energy signals before the final failure of the sample (Mogi 1962; Lockner and Byerlee 1977; Srinivasan *et al.* 2020). The AE signal at first produces less energy as it closes pre-existing cracks/microcracks and very negligible or no energy at the elastic deformation state since no sound waves are produced in this stage. This elastic deformation zone is found to be compulsorily present in all samples. It has also been observed that the field of crack closure (a–b line) in stress *vs.* AE diagram is present only in the D-charnockite gneiss (figure 9; samples B and E). This shows that the samples are neither dense nor intact. Comparing Mogi type response in the D-charnockite gneiss, the sample-B shows a Mogi type-II response but with a very short-spanned elastic state of deformation in the

Table 1. *Uniaxial compressive strength test of six samples from Gangavalli, Tamil Nadu.*

Sl. no.	Rock type	Sample	UCS σ_1 (MPa)	θ	σ_n	τ	C	Tensile
1	D-charnockite	B	19	10	0.57	3.25	2.91	–1.455
2		E	29	10	0.87	4.95	4.44	–2.22
Average			24	10	0.72	4.1	3.67	–1.83
3	Pt-charnockite	G	48.74	22	6.83	17	13.05	–6.52
4		K	45.67	4	0.22	3.18	3.05	–1.52
5		L	53.3	10	1.6	9.11	8.18	–4.09
6		M	34.61	14	2.02	8.12	6.95	–3.47
Average			45.58	12.5	2.17	9.41	8.15	–4.07

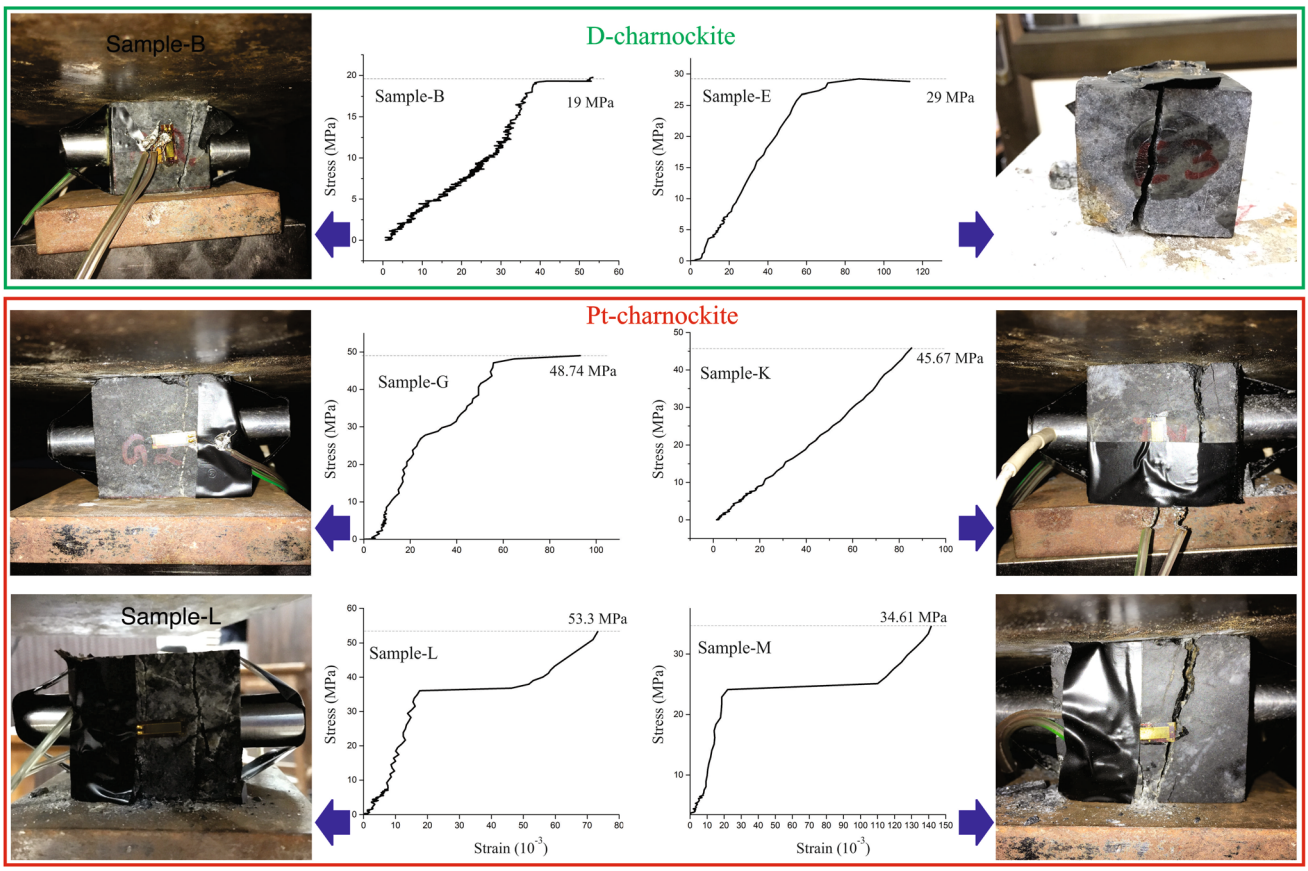

Figure 10. Stress *vs.* strain curves for each sample done by UCS test. The post-failure sample shows straight and axial parallel fracture surface.

stress *vs.* AE graph (figure 9; refer Mogi type graph in Mogi 1962). However, stable crack propagation field is missing in Sample-E indicating a brittle and very strong source rock. Both the D-charnockite gneisses are not dense and got deformed at the very initial stage of loading. The Sample-B and E, being unstable type (i.e., absent of stable crack propagation field) rock, immediately closes cracks at the onset of deformation and fails quickly. For all the D-charnockite gneisses, failure takes place at a very low stress range from 19 to 29 MPa (figure 10). All Pt-charnockite gneisses associated with pseudotachylite veins represent identical AE responses towards deformation (i.e., figure 9; Sample-G, K, L and M). These samples produce very low signal peaks at the beginning of the loading (figure 9), which corresponds to the linear elastic deformation zone (Mogi 1962). This elastic zone is identified to be started with a minimum of 13 MPa stress for Sample-K and maximum of 26 MPa stress for Sample-L. These Pt-charnockite gneisses refer to type-III curve of stress *vs.* AE graph, indicating a dense and stable rock. The stages of stable crack propagation are noticed in all the Pt-charnockite samples during loading (figure 11, Sample-M). At the initial stage, minor collateral cracks are produced and even become visible to the naked eye (figure 11). Later these cracks grow at tips and get connected, which is otherwise called as crack coalescences stage. The crack grows as long as the stress is applied to the samples where propagation can be controlled by the applied stress and hence, called stable fracture propagation phase (see figure 1 in Boyce *et al.* 1981). All the Pt-charnockite rocks show stable crack propagation phase during loading. Finally, the sample fails as a major crack with releasing energy. We also noticed that these cracks are produced at a high angle to the existing pseudotachylite plane orientation (nearly 40° with the compression direction) without following/reactivating its old plane (figure 11). This implies that the pseudotachylite melt act as a strong welding substance that seals weak/fracture surfaces and helps in gaining strength to the fault zone rocks. So, the possibilities of reactivation of slip surface may be very less in pseudotachylite accompanied fault zone rocks.

The rocks in the core of the fault zone suffer maximum damage due to concentration and uneven distribution of stress across the fault zone. However, the melt production along the fault interface adds more strength to the fault rock. It has been well observed in the UCS testing of D-charnockite gneiss and Pt-charnockite gneiss (i.e., stress at failure peaks is indicated by dash line in figure 10). The average value of maximum compression (σ_1) of Pt-charnockite gneiss is almost double than that of the D-charnockite gneiss (table 1). Now, these analyses have been compared with the strength of fresh charnockite gneiss obtained from different parts of the globe (references are given in table 2). The Mohr circle plot represents an overall idea of how strength variation occurs in fresh charnockite gneiss, D-charnockite gneiss and Pt-charnockite gneiss (figure 12a). For a fresh charnockite gneiss, the average $\sigma_1 = 139$ MPa (reference in table 2), breaking angle $\theta = 30$ and the average shear resistance $\tau = 30$ (obtained from the analysis of frictional shear resistance from a previous study, Behera *et al.* 2020) and angle of internal friction $\phi = 30$ (ideally taken for hard rock) have been used in equations (1–3). The rock does not break at the calculated cohesion $C = 49.53$, therefore, the Mohr circle has been rescaled

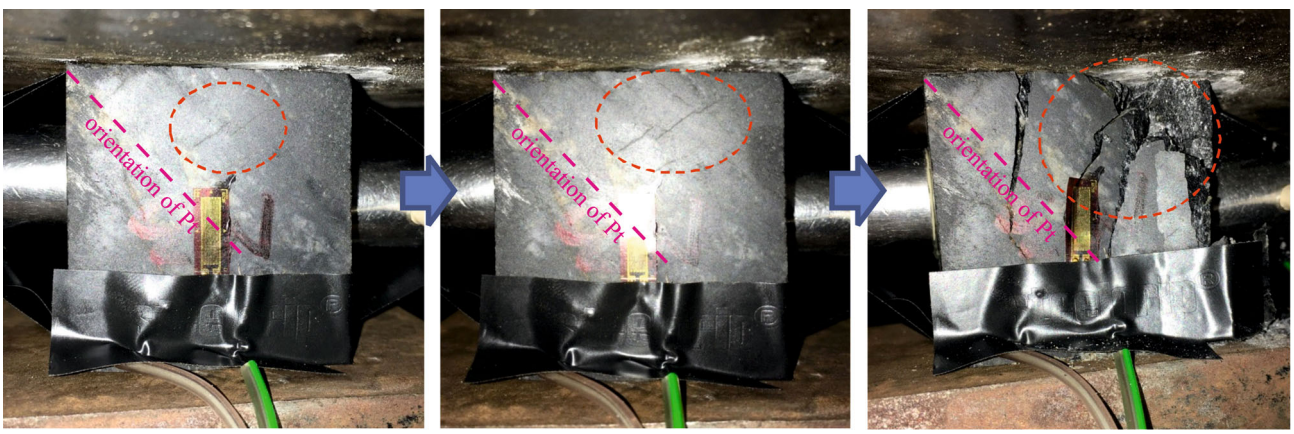

Figure 11. Photographs show the progress and coalescence of micro cracks in an *en ecelon* pattern orthogonal to the plane of pseudotachylite.

Table 2. *UCS value of fresh charnockite gneiss from literature study.*

Sl. no.	UCS (MPa)	Avg. UCS (MPa)	References
1	179.44–173.62	176.53	Ademila (2019)
2	111.50	111.50	Owoseni and Aro (2018)
3	138.98–167.52	153.25	Afolagboye *et al.* (2016)
4	63.7–167.7	115.7	Ekanayake *et al.* (2015)
5	82.86–165	112.33	Ademeso and Olaleye (2014)
6	104.2–231.6	167.9	Jayawardena (2011)
		Avg. 139.53	

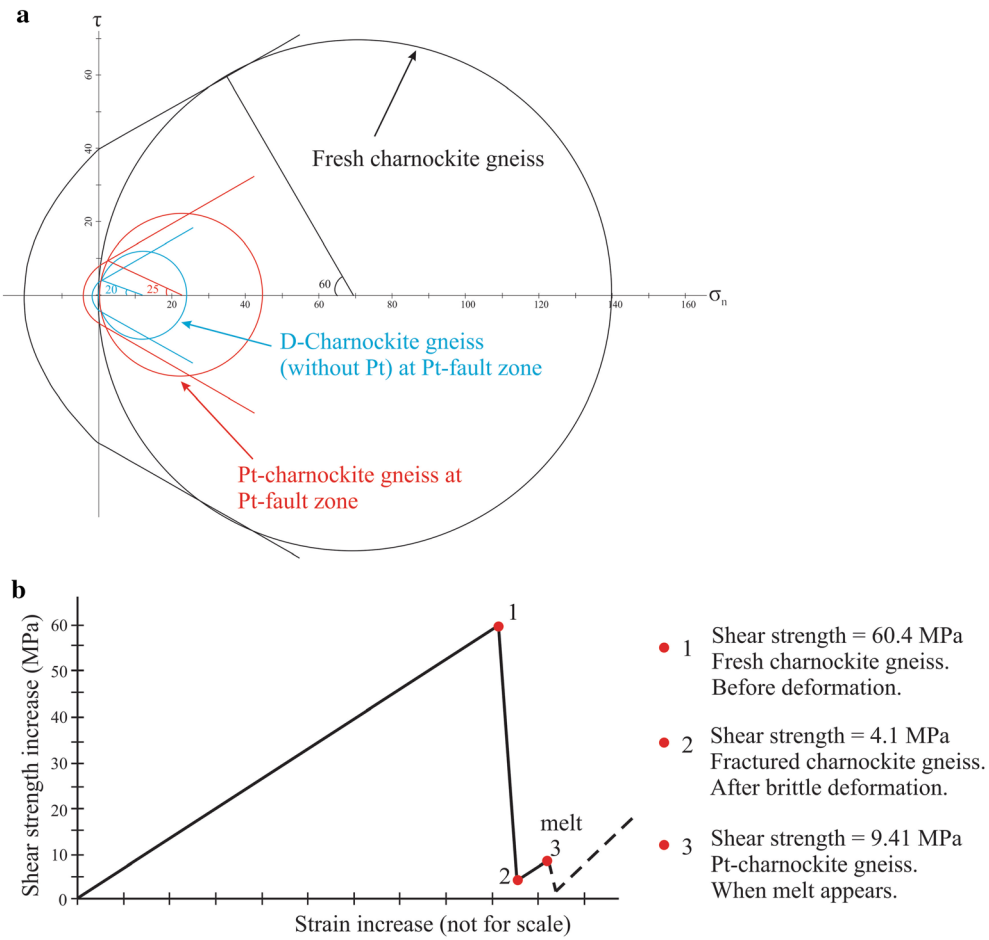

Figure 12. The plot shows a comparison of strength variation in different rock masses. **(a)** Mohr plot for UCS ($\sigma_3 = 0$) of fresh charnockite gneiss, deformed charnockite gneiss and pseudotachylite bearing charnockite and **(b)** shear stress of rocks drops after deformation and also increases to some extent by welding fracture openings.

(in Mohr plotter software) to possible failure at $C = 40.5$ (figure 12a). Here, the incipient fresh charnockite gneiss in the GFZ is considered as same as the fresh charnockite from worldwide (references are given in table 2) and has higher strength (i.e., average $\sigma_1 = 139$ MPa) and later, the strike–slip deformation causes the strength drop drastically up to an average of $\sigma_1 = 24$ MPa. However, the melt injection along the fault interface elevated the strength of the rocks (i.e., Pt-charnockite gneiss $\sigma_1 = 45.58$ MPa near-fault zone). Therefore, those rapid brittle faults produced with pseudotachylite melt strengthen the weak fault rocks to some extent immediately after the consolidation of the melt. Figure 12(b) reveals a stick-slip mechanism in the Gangavalli fault zone. For the onset of slip to happen, the tectonic stress needs to overcome the shear resistance of the

fresh charnockite gneiss, which is as high as 60.4 MPa (calculated using equation 1) (figure 12b). After deformation, the shear strength of the D-charnockite gneiss drops down to 4.1 MPa and then the melt increases cohesion of fault rocks, which made it stronger with increasing shear resistance up to 9.41 MPa. The further slip needs more shear stress (i.e., >9.41 MPa) to fail the block again. Pseudotachylites are often formed as pulses of melting rather than a continuous melting of a large volume. Stress drops during each melting and followed by building-up of stress due to consolidation of melt. This cyclic phenomenon of stress drops and building-up during each slip can be resembled with the stick-slip mechanism. Therefore, it can be inferred that a stick-slip mechanism could have played a role during pseudotachylite formation in the Gangavalli strike–slip faulting. Previous study suggests that σ_1 and σ_2 are horizontal and nearly equal in magnitude where the melt pressure (Pm) is in between σ_1 and σ_2 (i.e., $\sigma_3 << \sigma_2 \approx \text{Pm} \approx \sigma_1$; Behera *et al.* 2020). When the melt is produced along the fault interface, it drops the maximum stress (σ_1) of that area (e.g., because of the lubrication property of melt at the fault interface). As a result, σ_2 (previously $\sigma_2 < \sigma_1$) becomes the maximum stress ($\sigma_2 > \sigma_1$) and takes the place of σ_1 and similarly, σ_1 becomes σ_2. In this way, interchange of stresses occurs within subsequent slip as the fault progress with melting. This kind of pulse slipping is attributed to stick-slip faulting, where there is a time (in millisecond) pause between subsequent slip events. In agreement with the above observations, a flip-flop of principal stresses is believed to have occurred during Orosirian period (1.9 Ga, Behera *et al.* 2019) in the Gangavalli Fault zone.

7. Conclusion

Pseudotachylite vein-associated faults are very uncommon because of their seismogenic origin, which influence the rheological set-up of the fault zone rocks. Based on our analysis from the GFZ pseudotachylite, we have remarked some conclusive statements such as: (1) Pseudotachylite-bearing fault rocks are dense and stable unlike the pseudotachylite free fault rocks. (2) The melt under tremendous pressure had intruded into fracture openings and sealed them. As a result, subsequent failures are prevented along the same slip surface and therefore, new fracture planes are generated at some angle to it. (3) The post-seismic melting along the fault interface almost doubled the strength of the weak fault rocks and made them stronger and more stable. (4) Subsequent slip caused fluctuation of melt pressure along the fault surface and following which a flip-flop stress condition may be inferred in the area.

Acknowledgements

Authors convey their gratitude to Dr Trilok Nath Singh, who provided insight and guidance that greatly assisted the geotechnical study at the Department of Earth Sciences, Indian Institute of Technology Bombay (IIT Bombay). We also thank Dr Vinoth Srinivasan and Dr Bankim Mahanta for their suggestions and timely help during experimental work. We thank all the anonymous reviewers for their constructive reviews which greatly improved the manuscript and Dr Joydip Mukhopadhyay, Associate Editor for handling the manuscript.

Author statement

Bhuban Mohan Behera: Investigation, formal analysis, validation, visualisation, writing – original draft. Ashutosh Tripathy: Investigation, formal analysis, validation, visualisation. Tapas Kumar Biswal: Conceptualisation, validation, visualisation, writing – review and editing, supervision.

References

Ademeso O A and Olaleye B M 2014 Physico-mechanical characteristics of charnockitic rock of Akure, southwest Nigeria; *Gen. Sci. Res.* **2** 31–37.

Ademila O 2019 Engineering geological evaluation of some rocks from Akure, southwestern Nigeria as aggregates for concrete and pavement construction; *Geol. Geophys. Environ.* **45** 31.

Afolagboye L O, Talabi A O and Akinola O O 2016 Evaluation of selected basement complex rocks from Ado–Ekiti, SW Nigeria, as source of road construction aggregates; *Bull. Eng. Geol. Environ.* **75** 853–865.

ASTM 2001 Standard practices for preparing rock core specimens and determining dimensional and shape tolerances; Designation D4543.

Barker S L L 2005 Pseudotachylyte-generating faults in Central Otago, New Zealand; *Tectonophys.* **397** 211–223.

Beeler N M, Di Toro G and Nielsen S 2016 Earthquake source properties from pseudotachylite; *Bull. Seismol. Soc. Am.* **106** 2764–2776.

Behera B M, Thirukumaran V, Soni A, Mishra P K and Biswal T K 2017 Size distribution and roundness of clasts within pseudotachylytes of the Gangavalli shear zone, Salem, Tamil Nadu: An insight into its origin and tectonic significance; *J. Earth Syst. Sci.* **126** 46.

Behera B M, Waele B D, Thirukumaran V, Sundaralingam K, Narayanan S, Sivalingam B and Biswal T K 2019 Kinematics, strain pattern and geochronology of the Salem-Attur shear zone: Tectonic implications for the multiple sheared Salem–Namakkal blocks of the Southern Granulite terrane, India; *Precamb. Res.* **324** 32–61.

Behera B M, Thirukumaran V, Sharma N K and Biswal T K 2020 A preliminary study on earthquake source properties based on geochemistry, shear resistance and melt pressure of pseudotachylites, Gangavalli Fault, south India; In: *Structural geometry of mobile belts of the Indian Subcontinent*; Springer Cham, pp. 175–197.

Boyce G M, Koerner R M and McCabe W M 1981 Acoustic emission signature of various rock types in unconfined compression; ASTM International.

Chetty T R K, Yellappa T and Santosh M 2016 Crustal architecture and tectonic evolution of the Cauvery Suture Zone, southern India; *J. Asian Earth Sci.* **130** 166–191.

Collettini C, Niemeijer A, Viti C and Marone C 2009 Fault zone fabric and fault weakness; *Nature* **462** 907–910.

Di Toro G, Pennacchioni G and Teza G 2005 Can pseudotachylytes be used to infer earthquake source parameters? An example of limitations in the study of exhumed faults; *Tectonophys.* **402** 3–20.

Ekanayake E M T M, Herath H M J M K and Virajh Dias A A 2015 Empirical relationships of elastic modules and uniaxial strength of intact metamorphic rocks of Sri Lanka; *ICGE Colombo,* pp. 515–518.

Ishida T, Labuz J F, Manthei G, Meredith P G, Nasseri M H B, Shin K, Yokoyama T and Zang A 2017 ISRM suggested method for laboratory acoustic emission monitoring; *Rock Mech. Rock Eng.* **50** 665–674.

Jayawardena U D S 2011 Correlations between some strength properties of metamorphic rocks of Sri Lanka; *J. Geol. Soc. Sri Lanka* **14** 65–69.

Kirkpatrick J D, Shipton Z K and Persano C 2009 Pseudotachylytes: Rarely generated, rarely preserved, or rarely reported?; *Bull. Seismol. Soc. Am.* **99** 382–388.

Kirkpatrick J D and Rowe C D 2013 Disappearing ink: How pseudotachylytes are lost from the rock record; *J. Struct. Geol.* **52** 183–198.

Lockner D and Byerlee J 1977 Acoustic emission and creep in rock at high confining pressure and differential stress; *Bull. Seismol. Soc. Am.* **67** 247–258.

Mckenzie D and Brune J N 1972 Melting on fault planes during large earthquakes; *Geophys. J. Int.* **29** 65–78.

Mitchell T M, Virginia T, Giulio D T, Renner G and Sibson R H 2016 Fault welding by pseudotachylyte formation; *Geology* **44** 1059–1062.

Mogi K 1962 Study of elastic shocks caused by the fracture of heterogeneous materials and its relation to earthquake phenomena; *Bull. Earthq. Res. Inst., University of Tokyo* **40** 125–173.

Owoseni J O and Aro S O 2018 Effect of parent rock on liquid limits and compaction characteristics of residual lateritic soils; *Iconic Res. Eng. J.* **2** 69–74.

Phillips N J, Rowe C D and Ujiie K 2019 For how long are pseudotachylytes strong? Rapid alteration of basalt-hosted pseudotachylytes from a shallow subduction complex; *Earth Planet. Sci. Lett.* **518** 108–115.

Proctor B and Lockner D A 2016 Pseudotachylyte increases the post-slip strength of faults; *Geology* **44** 1003–1006.

Ramakrishnan M and Vaidyanadhan R 2008 *Geology of India*; GSI Publications.

Sarkar A and Chattopadhyay A 2020 Microstructure and geochemistry of pseudotachylyte veins from Sarwar–Junia Fault Zone, India: Implications for frictional melting process in a seismic fault zone; *Geol. J.* **55(12)** 7687–7715.

Sibson R H 1975 Generation of pseudotachylyte by ancient seismic faulting; *Geophys. J. Roy. Astron. Soc.* **43** 775–794.

Sibson R H, Toy V G and Abercrombie R 2006 The habitat of fault-generated pseudotachylyte: Presence *vs.* absence of friction-melt; *Geophys. Monogr. Am. Geophys. Union* **170** 153.

Smith S A F, Tesei T, Scott J M and Collettini C 2017 Reactivation of normal faults as high-angle reverse faults due to low frictional strength: Experimental data from the Moonlight Fault Zone, New Zealand; *J. Struct. Geol.* **105** 34–43.

Srinivasan V, Tripathy A, Gupta T and Singh T N 2020 An investigation on the influence of thermal damage on the physical, mechanical and acoustic behaviour of Indian Gondwana shales; *Rock Mech. Rock Eng.* **53** 2865–2885.

Sundaralingam K, Waele B D, Thirukumaran V, Thakur S S, Mahadani T and Biswal T K 2013 Deformation, metamorphism and geochronology of the Palaeoproterozoic Salem-Namakkal fold thrust belt and implication for the Gondwanaland continental assembly; *Int. J. Geol. Earth Environ. Sci.* **2** 266–283.

Tripathy A, Srinivasan V, Maurya K K, Sirdesai N and Singh T N 2018 Acoustic and Failure behaviour of gondwana shale under uniaxial compressive and indirect Brazilian tensile loading – an experimental study; In: *ISRM Regional Symposium-Eurock*; *Int. Soc. Rock Mech. Rock Eng.*, pp. 687–693.

Corresponding editor: Joydip Mukhopadhyay